JOURNAL OF MATERIALS SCIENCE 31 (1996) 921–925

Undercooling and supersaturation of alloying elements in rapidly solidified Al–8.5% Fe–1.2% V–1.7% Si alloy

S. HARIPRASAD, S. M. L. SASTRY, K. L. JERINA
Materials Research Laboratory, Washington University, St Louis, MO 63130 USA

Dispersion-strengthened Al–8.5% Fe–1.2% V–1.7% Si alloy was produced by inert gas atomization and atomized melt deposition processes. Differential scanning calorimetry was used to estimate the extent of undercooling in the alloy powders as a function of powder size and in the atomized melt-deposited alloy as a function of process parameters. The estimated undercooling was found to be a strong function of powder size and processing conditions and varied from 380–200 °C. Alloy powders of diameter greater than 180 μm did not experience any undercooling during solidification. X-ray diffraction analysis was performed to study the dependence of supersaturation of alloying elements and metastable phase formation on the extent of undercooling. When the undercooled alloy was heated to about 400 °C, formation of $Al_{12}(Fe, V)_3Si$ phase with b c c crystal structure from the supersaturated matrix was observed.

1. Introduction

Inert gas atomization (IGA) [1, 2], atomized melt deposition (AMD) [3] and planar flow casting (PFC) [4] are some of the commonly employed rapid solidification (RS) techniques to produce high-performance aluminium alloys. In an RS process, rapid heat extraction from the metallic melt leads to undercooling below the thermodynamic crystallization temperature. The undercooling controls the nucleation, phase selection and the metastable structures formed during rapid solidification processing [5, 6]. In the IGA process, a liquid alloy stream is disintegrated into a spray of droplets by inert gas at high pressure and the droplets are quenched by inert gas to produce powders. The undercooling and cooling rate experienced by droplets during rapid solidification are strong functions of droplet size. In the AMD process, the spray of droplets produced by inert gas atomization are collected on to a substrate of suitable geometry to produce near net shape products. Process parameters, such as melt superheat, metal to gas flow rate ratio, and substrate to nozzle distance, control the undercooling and cooling rate of the deposit. In the PFC process, melt spinning produces ribbons of about 30 μm thickness, resulting in a cooling rate of 10^6 K s^{-1}. Using the PFC process, Allied Signal Inc. [4] commercially produces dispersion-strengthened Al–8.5% Fe–1.2% V–1.7% Si alloy, a promising alloy system for elevated temperature application. In the present investigation, this alloy was produced by IGA and AMD processes. Differential scanning calorimetry (DSC) was used to estimate the extent of undercooling and X-ray diffraction analysis was carried out to determine the dependence of supersaturation of solute elements in the alloy on the extent of undercooling. Based on the analysis of electron microscopy data and the established relationship between cooling rates and the secondary dendrite arm spacings, cooling rates were estimated for the alloy.

2. Experimental procedure

An alloy of nominal composition Al–8.5% Fe–1.2% V–1.7% Si was produced by IGA and AMD processes. The processing details of IGA and AMD are described elsewhere [3]. The alloy processed by PFC [4] was procured from Allied-Signal Inc., in the form of rolled rectangular sheets, 6 mm thick. The alloy powder was examined by optical and scanning electron microscopy and the secondary dendrite arm spacings were measured to estimate the cooling rates achieved as a function of the powder size. The alloy powder was sieved to obtain powders of various size fractions. The size fraction less than 30 μm and the fraction of 180 μm $< d <$ 250 μm were annealed in a vacuum of 10^{-6} torr (1 torr = 133.322 Pa) at 430 °C for 24 h. By varying process parameters such as substrate to nozzle distance, metal to gas flow rate ratio and pouring temperature, Al–8.5% Fe–1.2% V–1.7% Si alloy with varying grain and dispersoid size was produced using the AMD process. Cooling rates for the AMD alloys were estimated using a procedure discussed elsewhere [3]. The atomized melt-deposited alloy was tested in the as-deposited condition and after thermo-mechanical processing. The as-deposited condition refers to the AMD alloy with no subsequent processing. The alloys were thermomechanically processed by hot-isostatically pressing at 410 °C and

0022–2461

203 MPa for 4 h and extruding into 6 mm diameter rods at 400 °C with an extrusion ratio of 16:1 [3]. The powder alloys and bulk AMD alloys in the as-deposited condition were subjected to DSC scans in a nitrogen atmosphere at 40 °C min^{-1} from 110–440 °C using a Perkin–Elmer DSC-4. X-ray diffraction analyses were performed on gas-atomized powders in as-processed and annealed conditions and on AMD deposits in as-deposited and extruded conditions, to identify the phases produced under different rapid solidification conditions.

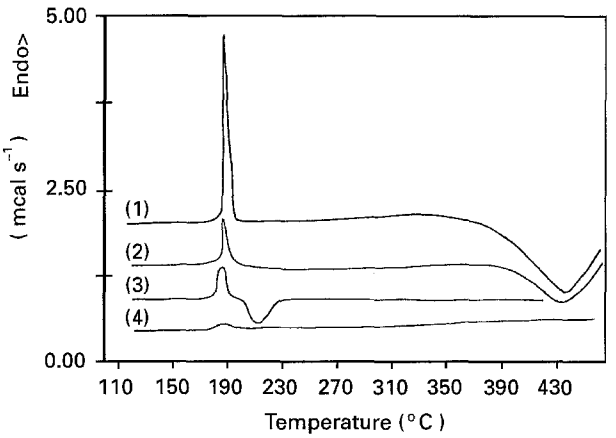

Figure 2 DSC traces for Al–8.5% Fe–1.2% V–1.7% Si alloy powder of different size fractions processed by the inert gas atomization process. (1) $< 30\ \mu m$, (2) $30\ \mu m < d < 60\ \mu m$, (3) $125\ \mu m < d < 180\ \mu m$, (4) $180\ \mu m < d < 250\ \mu m$.

3. Results and discussion

Fig. 1a–f show the microstructures of the alloy produced by IGA and AMD processes. The size of the dispersoids is a strong function of the powder size and the cooling rate in the case of gas-atomized powders. In the alloy produced by AMD, the distribution and size of the dispersoids are also dependent on the cooling rate which, in turn, depends on the processing conditions [3]. The grain size and dispersoid diameter in the case of AMD alloy-1 were about 1 μm and 70 nm, respectively. In the case of AMD alloy-2, the grain size and dispersoid diameter were about 2 μm. Fig. 2 shows the results of the DSC experiments for the gas-atomized powder alloy. The onset temperature for the exotherms, in the case of the powder alloy, is dependent on the powder size, while the onset temperature for the endotherm is independent of the powder size. The exotherms are absent in the gas-atomized alloy for powder sizes greater than 180 μm. Fig. 3 shows the DSC traces obtained for the AMD alloys. The exotherm in AMD alloy 1 is observed at about 310 °C, and such an exotherm is absent in the case of AMD alloy 2. Fig. 4a–c show the X-ray diffraction results for PFC alloy sheet and the IGA alloy in as-processed and annealed conditions. The diffraction

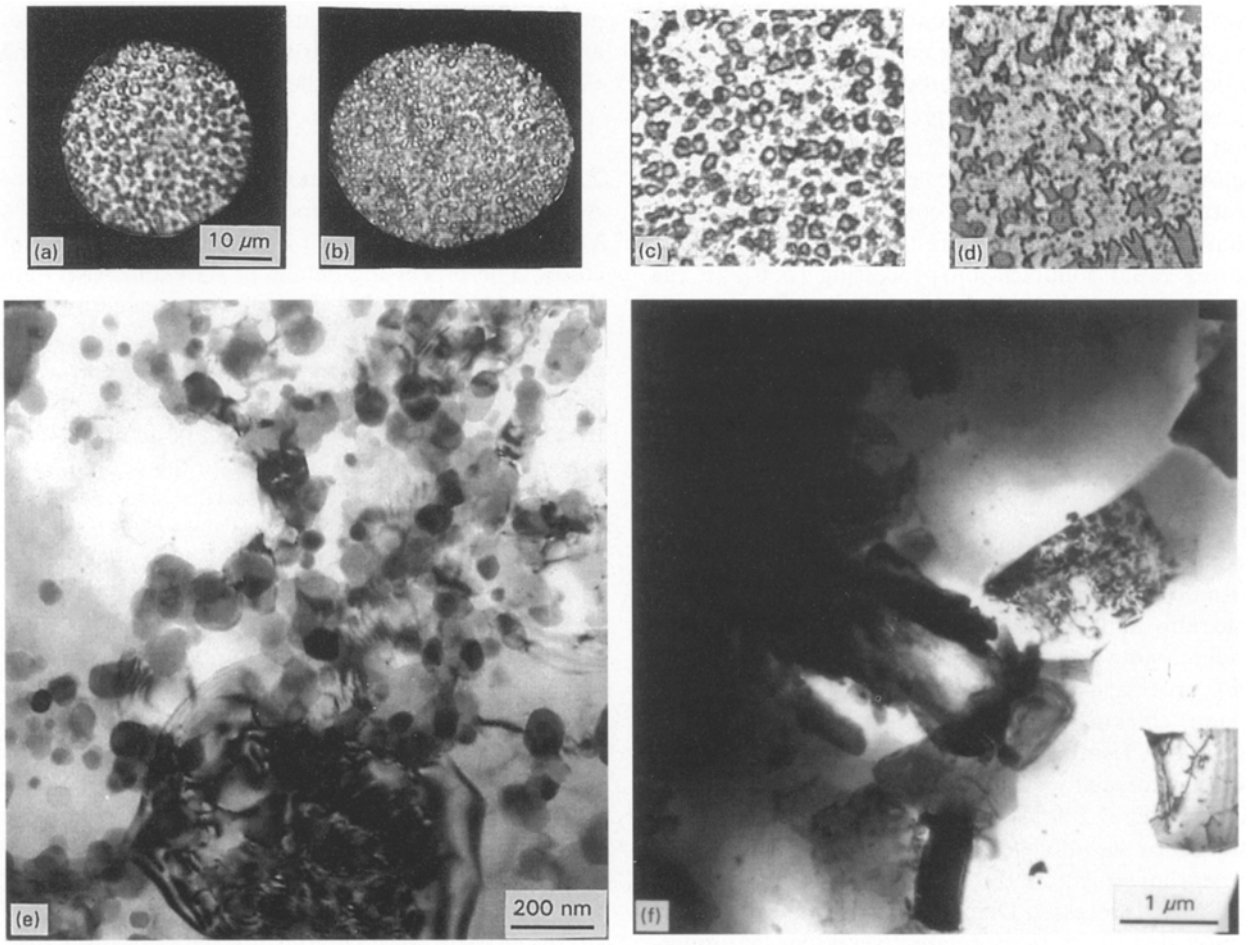

Figure 1 Microstructures of Al–8.5% Fe–1.2% V–1.7% Si alloy produced by (a–d) inert gas atomization and (e, f) atomized melt deposition processes. (a) $d < 30\ \mu m$, (b) $30\ \mu m < d < 60\ \mu m$, (c) $125\ \mu m < d < 180\ \mu m$, (d) $180\ \mu m < d < 250\ \mu m$, (e) AMD alloy 1, (f) AMD alloy 2.

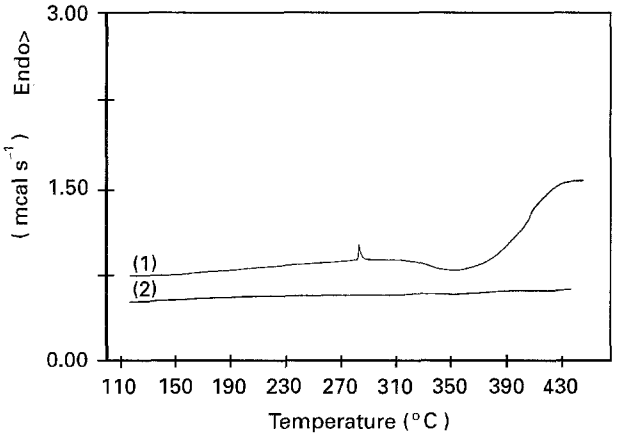

Figure 3 DSC traces for Al–8.5% Fe–1.2% V–1.7% Si alloy produced by the atomized melt deposition process. (1) Alloy 1, (2) alloy 2.

pattern indicates the differences in the phases present for the powder alloy for different powder sizes in as-processed and annealed conditions. The X-ray diffraction patterns for the AMD alloys are shown in Fig. 5a and b. Table I lists the estimated cooling rates and the undercooling experienced by the inert gas atomized alloy and AMD alloy based on the analysis of microscopy and DSC experiments.

During rapid solidification processing, the alloy is cooled through a non-equilibrium phase region leading to the formation of metastable phases and supersaturation of the solute elements in the solid solution. When the rapidly solidified alloy is reheated, as in the case of the DSC experiment, the phases allowed by non-equilibrium kinetics will undergo solid-state transformation and the supersaturated alloying elements in the matrix precipitate out to form new metastable phases. This results in the exothermic peaks as observed in the case of gas-atomized and AMD alloy and confirms the existence of non-equilibrium phases and the matrix supersaturated with solute elements. The onset temperature of exotherms, therefore, is a direct measure of the amount of undercooling experienced by the alloy during processing [7]. The absence of exotherms in the gas-atomized alloy for the powder size greater than 180 μm indicates insufficient undercooling and the absence of supersaturation of alloying elements in the matrix. As a result, the precipitation of metastable phases is not seen in the case of coarser powders of size greater than 180 μm. Similarly, the

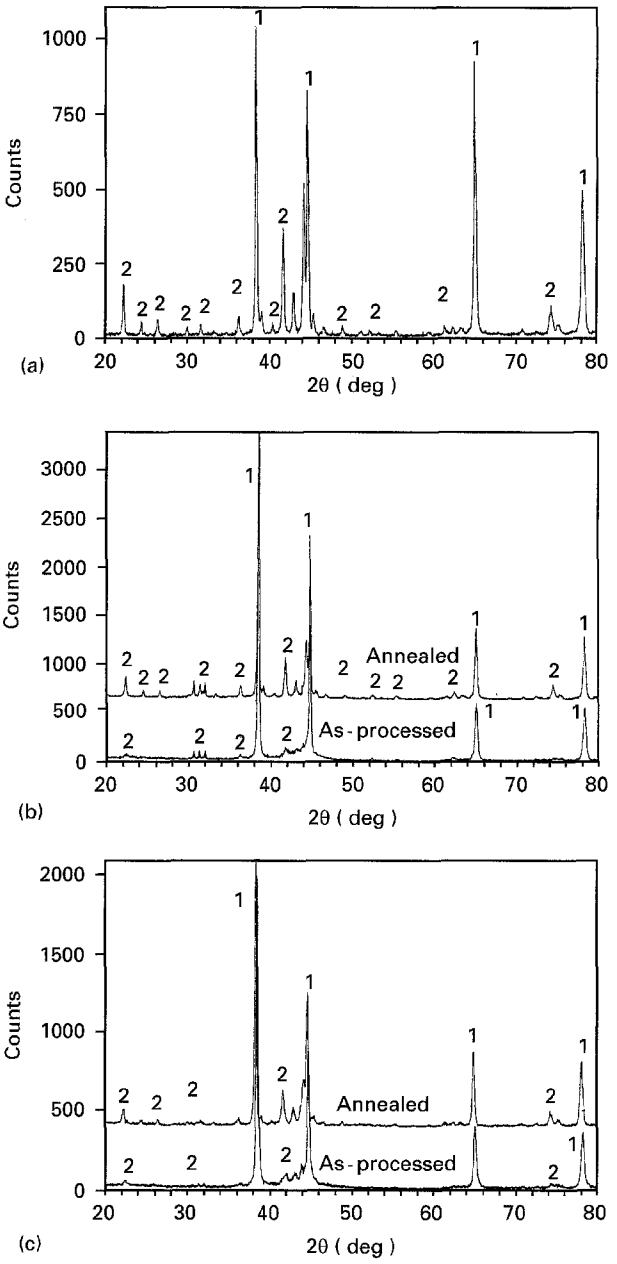

Figure 4 X-ray diffraction pattern for Al–8.5% Fe–1.2% V–1.7% Si alloy produced by (a) planar flow casting, (b) inert gas atomization of powder size < 30 μm, and (c) inert gas atomization of powder size fraction of 180 μm $< d <$ 250 μm. (1) Aluminium, (2) $Al_{12}(Fe, V)_3Si$ phase.

TABLE I Estimated cooling rates and undercooling

Alloy	Cooling rate (K s^{-1})	Heterogeneous undercooling (K)	Calculated homogeneous undercooling (K)
Powder alloy size fraction (μm)			
$d < 30$	10^5	380	497 (30 μm)
$30 < d < 60$	10^4 to 4×10^4	380	479 (60 μm)
$125 < d < 180$	10^3 to 5×10^3	200	456 (180 μm)
$180 < d < 250$	3×10^2 to 10^3	–	450 (250 μm)
AMD alloys			
Alloy 1	8.5×10^3	310	–
Alloy 2	5×10^2 to 2.5×10^3	–	–

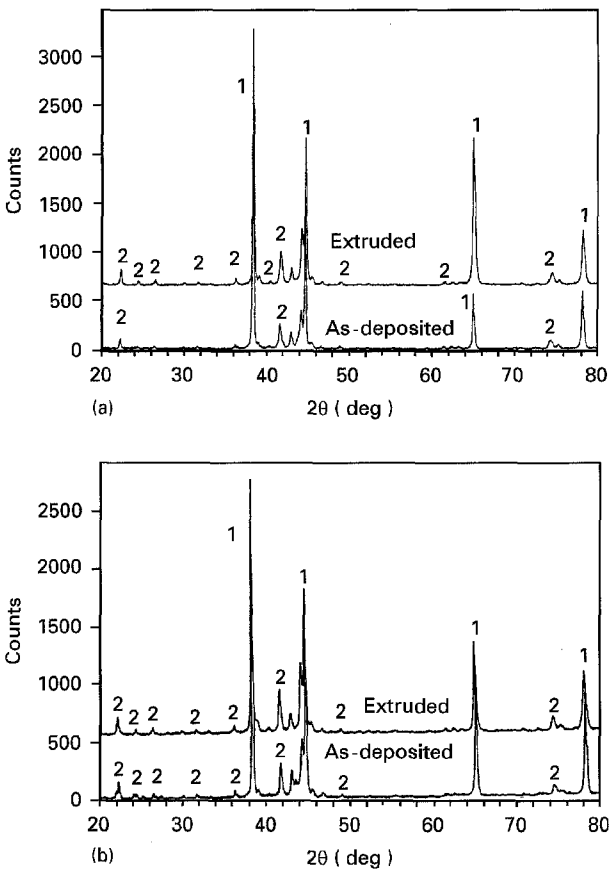

Figure 5 X-ray diffraction pattern for Al–8.5% Fe–1.2% V–1.7% Si alloy produced by the atomized melt deposition process. (a) AMD alloy 1, (b) AMD alloy 2. (1) Aluminium, (2) $Al_{12}(Fe, V)_3Si$ phase.

supersaturation level in AMD alloy 1 is more than that of AMD alloy 2.

The undercooling necessary for the homogeneous nucleation conditions is given by the following expression according to Hirth [8]

$$\Delta T_c^2 = \frac{(16\pi\sigma_m^3 \nu^2 T_l^2)}{3kT_n\Delta H_f^2 \ln\left[d^3 10^{-3}\left(\frac{2\sigma_m T_l \nu}{\Delta H_f a \Delta T_c}\right)^2\left(\frac{a}{\nu}\right)D\left(\frac{\Delta T_c}{\dot{T}}\right)\right]} \quad (1)$$

where T_n is the nucleation temperature, $\dot{T}$ is the cooling rate and d is the diameter of the droplet. As seen from this expression the extent of undercooling depends on the droplet size, cooling rate, latent heat of fusion and other thermo-physical properties. The above equation was solved with a Newton–Raphson algorithm with the thermophysical properties listed in Table II. The undercooling for homogeneous nucleation conditions for several droplet sizes were calculated and are shown in Table I. However, heterogeneous nucleation due to the presence of nucleation sites such as impurities or extraneous surfaces, governs the solidification process in the case of droplet sizes considered. The extent of undercooling for heterogeneous nucleation conditions is less than that for homogeneous nucleation conditions. Therefore, the estimated undercooling levels for heterogeneous nucleation conditions shown in Table I are lower

TABLE II Thermo-physical properties

Atom volume, $\nu = 2.34 \times 10^{-29}$ m^3
Atom diameter, $a = 2.86 \times 10^{-10}$ m
Solid-liquid surface energy, $\sigma_m = 0.109$ J m^{-2}
Liquidus temperature, $T_l = 933$ K
Latent heat of fusion, $\Delta H_f = 397\,746$ J kg^{-1}
Diffusion coefficient, $D = 3 \times 10^{-9}$ m^2 s^{-1}
Boltzman's constant, $k = 1.38 \times 10^{-23}$ J at^{-1} K^{-1}

than the undercooling values calculated using Equation 1 for homogeneous nucleation conditions. The undercooling levels for homogeneous nucleation conditions decrease gradually when droplet diameter increases from 30 μm to 250 μm according to Equation 1. But the undercooling levels for heterogeneous nucleation conditions decrease drastically as seen from Table I when droplet size increases from 30 μm to 250 μm because there is an exponential increase of nuclei as the droplets become coarser.

The endothermic peaks observed in the DSC traces of the powder alloy in all the size fractions may be due to a dissolution reaction. Also, the size of the endothermic peak is a function of the powder size. Further work is in progress to investigate the cause for this endothermic reaction and the dependence of the peak size on the powder size.

The $Al_{12}(Fe, V)_3Si$ phase with the b c c crystal structure, precipitates out from the supersaturated matrix when the Al–8.5% Fe–1.2% V–1.7% Si alloy is heated to about 425 °C [9, 10]. Fig. 4a shows the presence of precipitated $Al_{12}(Fe, V)_3Si$ phase in the case of PFC alloy sheet which was hot isostatically pressed and extruded at 420 °C using communited planar flow-cast ribbons [4]. In the case of finer as-processed powder alloy of size less than 30 μm, where supersaturation levels are high, the presence of $Al_{12}(Fe, V)_3Si$ phase is less evident as seen in Fig. 4b. However, on annealing at 430 °C, the $Al_{12}(Fe, V)_3Si$ phase precipitates out and hence the presence of $Al_{12}(Fe, V)_3Si$ phase peaks increase as seen in Fig. 4b. In as-processed coarser powder alloy of size greater than 180 μm, supersaturation of alloying elements is low owing to the level of undercooling achieved during processing. As seen from the Fig. 4c, new phase formation is not seen in the X-ray diffraction pattern after annealing except for the peaks of $Al_{12}(Fe, V)_3Si$ phases which coarsen and are already present before annealing. Similarly, in the case of AMD alloy 1, where the supersaturation levels were higher, peaks of precipitated $Al_{12}(Fe, V)_3Si$ phase are more evident than in the case of AMD alloy 2 where the supersaturation levels were not high.

4. Conclusion

The estimated undercooling for the Al–8.5% Fe–1.2% V–1.7% Si alloy produced by IGA and AMD varied from 380–200 °C. Atomized powders of diameters greater than 180 μm, and AMD alloy deposits processed with lower cooling rates, undergo solidification without any appreciable undercooling. X-ray diffraction analysis of the as-processed and annealed alloy

showed that the supersaturation of alloying elements is directly dependent on the undercooling experienced during solidification of the alloy.

References

1. N. J. GRANT, in "Proceedings of symposium on High Strength Powder Metallurgy Aluminum Alloys", edited by M. J. Koczack and G. J. Hilderman (AIME, Warrendale, PA, 1982) p. 3.
2. R. E. LEWIS and E. A. STARKE Jr, in "Proceedings of a Symposium on Mechanical Behavior of Rapidly Solidified Materials," edited by S. M. L. Sastry and B. A. MacDonald (AIME Warrendale, PA, 1986) p. 151
3. S. HARIPRASAD, S. M. L. SASTRY, K. L. JERINA and R. J. LEDERICH, *Metall. Trans.* **24 A** (1993) 865.
4. D. J. SKINNER, R. L. BYE, D. RAYBOULD and A. M. BROWN, *Scripta Metal. Mater.* **20** (1986) 867.
5. F. SPAPEAN and D. TURNBULL, in "Proceedings of the 4th Conference on Rapid Solidification Processing, Principles and Technologies", edited by R. Mehrabian and P. A. Parish (Claitor's, Baton Rouge, LA, 1988) p. 1.
6. W. J. BOETTINGER and J. H. PERPEZKO, in "Proceedings of a TMS-AIME regional meeting on Rapidly Solidified Crystalline Alloys", edited by S. K. Das, B. H. Kear and C. M. Adam (AIME, Warrandale, PA, 1985) p. 21.
7. C. M. ADAM, V. R. V. RAMANAN and D. J. SKINNER, in "Proceedings of Symposium on Undercooled Alloy Phases", edited by E. W. Collings and C. C. Koch (AIME, Warrandale, PA, 1986) p. 59.
8. J. P. HIRTH, *Metall. Trans.* **9A** (1978) 401.
9. D. J. SKINNER, R. L. BYE, D. RAYBOULD, A. M. BROWN and M. S. ZEDALIS, in "Proceedings of Symposium on Processing of Structural Metals by Rapid Solidification", edited by F. H. Froes and S. J. Savage (AIME, Warrandale, PA, 1987) p. 291.
10. N. J. KIM, *Int. J. Rapid Solid.* **6** (1991) 175.

Received 25 October 1994
and accepted 28 April 1995